J. Phys.: Condens. Matter 6 (1994) 1333–1344. Printed in the UK

High-pressure crystal chemistry and phase transition of $RbTi_2(PO_4)_3$

Robert M Hazen†, David C Palmer†§, Larry W Finger†, Galen D Stucky‡, W T A Harrison‡ and T E Gier‡

† Geophysical Laboratory and Center for High-Pressure Research, 5251 Broad Branch Road NW, Washington, DC 20015-1305, USA

‡ Department of Chemistry, University of California, Santa Barbara, CA 93106-9510, USA

Received 17 September 1993, in final form 8 November 1993

Abstract. Unit-cell parameters of $RbTi_2(PO_4)_3$, a framework structure (space group $R\bar{3}c$) with alternating corner-linked Ti octahedra and P tetrahedra that define six-coordinated alkali cation sites, were determined at eight pressures from 0.0 to 6.2 GPa, and crystal structure refinements were obtained at 0.0 and 6.2 GPa. The structure remains dimensionally rhombohedral at all pressures, with the a axis more than four times more compressible than c. Compressibilities of both axes increase abruptly above about 1.7 GPa; the bulk modulus decreases from 104(3) GPa ($K' = 4$) to approximately 60 GPa. Furthermore, the appearance of reflections that violate the c glide-plane symmetry above 1.7 GPa signals the occurrence of a reversible phase transition involving distortion of the framework. From the pressure dependence of the intensities of critical x-ray reflections, the phase transition is revealed as being continuous and close to second order in character. Structure refinements of the 6.2 GPa data reveal $R3$ symmetry, an acentric space group, for the high-pressure form. Average Ti–O–P angles decrease from 151.5 to 140° between room pressure and 6.2 GPa. These changes result in a coordination change for Rb from one centric six-coordinated site (Rb–O = 2.855 Å) at room pressure, to two symmetrically distinct acentric 12-coordinated sites (mean Rb–O $\simeq$ 3.01 Å) at 6.2 GPa.

1. Introduction

Reversible high-pressure phase transitions involving distortion of a corner-linked polyhedral network are common in silicates, phosphates, and other materials with tetrahedral and octahedral frameworks of trivalent, tetravalent, and pentavalent cations (Megaw 1973, Hazen and Finger 1979). Of special interest are the alkali titanophosphates, including compounds with the acentric $KTiPO_5$ structure with corner-linked frameworks of octahedral Ti and tetrahedral P, which display strongly non-linear optical behaviour and are used as second-harmonic generators (Zumsteg *et al* 1976).

At room pressure $RbTi_2(PO_4)_3$ occurs in a closely related structure (centric, $R\bar{3}c$). The structure of $RbTi_2(PO_4)_3$ and several other isomorphs was reported by Masse (1970), who found that each Ti octahedron is linked to six P tetrahedra, while each tetrahedron is linked to four octahedra—the same framework topology that is observed in garnet. Alkali cations occupy large cavities defined by the Ti–P net. A polyhedral drawing of the $RbTi_2(PO_4)_3$

§ Present addresses: Emmanuel College, Cambridge CB2 3AP, UK and Department of Earth Sciences, University of Cambridge, Downing Street, Cambridge CB2 3EQ, UK.

0953-8984/94/071333+12$07.50

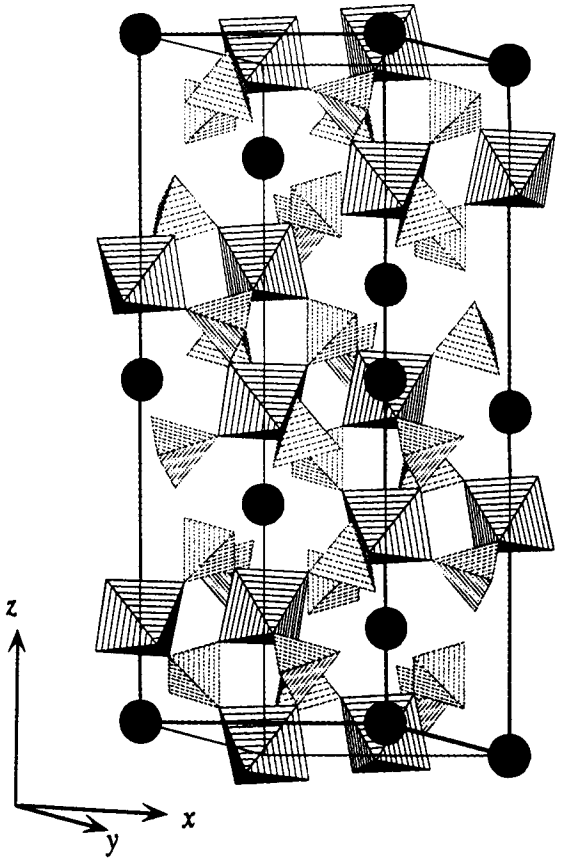

Figure 1. A polyhedral representation of the $RbTi_2(PO_4)_3$ structure illustrates the corner-linked distribution of alternating Ti octahedra and P tetrahedra—a topology identical to that of garnet. Black circles represent Rb ions. The unit cell, outlined in its hexagonal setting, has $a = 8.29$ and $c = 23.56$ Å.

structure (figure 1) reveals its framework topology and the unit cell (in the hexagonal setting: $a = 8.29$ Å; $c = 23.56$ Å).

High pressure provides a means for us to sample a progression of structural distortions and variants with potentially new and useful properties—materials that might then be duplicated at room conditions by appropriate compositional changes. This strategy is similar to that of inducing structural changes by heating, but pressure may cause volume changes an order of magnitude greater than temperature. Of special interest in the case of framework structures are reversible phase transitions involving structural distortions of corner-linked polyhedral arrays. Most framework structures studied at pressures to several GPa display one or more of these transitions, in which significant volume reduction is achieved without bond breaking by decreasing average cation–O–cation bond angles. Such bond bending, however, commonly leads to a reduction in symmetry, often with an increase in compressibility as additional tilting degrees of freedom become possible. Well known examples include transitions in silica polymorphs (Palmer and Downs 1991, Palmer *et al* 1992, Downs and Palmer 1993, Palmer and Finger 1994), perovskites and related compounds (Schirber *et al* 1984, Hazen and Finger 1984a, Wang *et al* 1991), $NaTiPO_5$ and related compounds (Allan *et al* 1992, Allan and Nelmes 1992), feldspars (Hazen 1976, Angel 1992), and zeolites (Hazen and Finger 1979, 1984b, Hazen 1983).

Given the varied and interesting high-pressure behaviour of these other framework compounds, as well as the importance of framework Ti phosphates in non-linear optical

applications, we undertook this study to describe high-pressure structural variations and properties of $RbTi_2(PO_4)_3$.

2. Experimental details

Colourless, transparent crystals of $RbTi_2(PO_4)_3$ up to 0.5 mm were synthesized hydrothermally (Phillips *et al* 1992). An equidimensional single crystal approximately 0.1 mm in diameter was selected for study at room pressure. We obtained room-pressure x-ray data using a Rigaku AFC-5 diffractometer with rotating anode generator and graphite monochromatized Mo $K\alpha_1$ radiation ($\lambda = 0.7093$ Å). The crystal has a rhombohedral unit cell (space group $R\bar{3}c$; $Z = 8$; $a = 8.2890(10)$; $c = 23.563(2)$ Å; $V = 1402.06(36)$ Å^3; calculated density = 3.31 g cm^{-3}; $\mu_l = 73.0$ cm^{-1}). Four octants of intensity data were measured to $2\theta = 60°$ ($\sin\theta/\lambda = 0.70$), using ω step scans, yielding 2901 measured reflections including standards. These data were averaged according to Laue symmetry $\bar{3}m$ for all reflections, to give 459 symmetrically independent structure factors (internal agreement 3.3%), of which all but one were observed ($I \geqslant 2\sigma$).

High-pressure x-ray diffraction data were obtained on a crystal mounted in a Merrill–Bassett-type diamond anvil cell (Merrill and Bassett 1974) as modified by Hazen and Finger (1982). A 4:1 mixture of methanol:ethanol was employed as the pressure-transmitting medium. The pressure cell was mounted on a Picker automated four-circle diffractometer with Nb-filtered Mo radiation. Unit-cell parameters were obtained by centring from 16 to 20 reflections with $30° \leqslant 2\theta \leqslant 45°$ in eight equivalent positions, following the procedure of King and Finger (1979). Initial unit-cell refinements were made without constraints (i.e. as triclinic) to test for deviations from rhombohedral symmetry. Unit-cell parameters at all pressures were within two estimated standard deviations of ideal dimensions, and final parameters recorded in table 1 were calculated in the hexagonal setting with appropriate constraints (Ralph and Finger 1982).

Table 1. Unit-cell parameters of $RbTi_2(PO_4)_3$ (hexagonal setting) versus pressure. $\sigma(a)$, $\sigma(c)$, $\sigma(V)$ are the one-sigma errors in the a and c parameters and the unit-cell volume, respectively, as calculated from least-squares refinement with hexagonal constraints.

P (GPa)	a (Å)	$\sigma(a)$ (Å)	c (Å)	$\sigma(c)$ (Å)	V (Å^3)	$\sigma(V)$ (Å^3)
0.00	8.2890	0.0010	23.563	0.002	1402.06	0.36
0.29	8.2790	0.0010	23.554	0.003	1398.14	0.38
0.77	8.2650	0.0020	23.545	0.005	1392.88	0.74
1.36	8.2450	0.0010	23.531	0.003	1385.33	0.38
1.66	8.2290	0.0010	23.523	0.002	1379.49	0.36
2.11	8.1835	0.0009	23.504	0.001	1363.17	0.31
3.06	8.1116	0.0007	23.472	0.001	1337.50	0.24
6.21	7.9200	0.0008	23.373	0.001	1269.68	0.26
0.00	8.2895	0.0010	23.557	0.002	1401.95	0.28

X-ray measurements were performed at eight increasing pressures, as well as at room conditions following the highest-pressure measurements. Pressure calibration was achieved by measuring the laser-induced fluorescence of ruby chips less than 10 μm in diameter scattered throughout the sample chamber, and correlating with the ruby pressure scale of Mao *et al* (1978). We took particular care to ensure a consistent and relatively accurate pressure calibration. Ruby fluorescence spectra were fitted using least-squares profile

refinement, fitting Lorentzian functions to the R1 and R2 peaks. Absolute calibration was achieved with reference to a room-pressure ruby standard, measured in an identical manner to the sample at pressure. In these experiments, pressure gradients were all less than the experimental uncertainty of ±0.05 GPa.

A full set of intensity data was collected at 6.2 GPa, the highest pressure attained in these experiments. All accessible reflections to $\sin\theta/\lambda \leqslant 0.7$ were collected on a Picker automated four-circle diffractometer with Nb-filtered Mo radiation. A total of 1428 reflections (including standards) were collected, corrected for absorption by the crystal and the diamond cell, and averaged both according to Laue group $\bar{3}m$ (internal agreement 2.6%) and $\bar{3}$ (internal agreement 2.2%). We thus assumed Laue group $\bar{3}$, which yielded 504 symmetrically independent data, of which 394 were observed.

3. Results

3.1. Unit-cell compression

Unit-cell parameters at nine pressures, including room pressure before and after the experiments, are reported in table 1 and illustrated in figure 2. Compression is highly anisotropic, with the a axis approximately four times more compressible than the c axis. Axial lengths for low pressure from between 0 and 1.7 GPa may be represented by linear functions of pressure:

$$a = 8.2895(18) - 0.0349(17)P \qquad c = 23.5625(7) - 0.0237(6)P.$$

Between 1.7 and 6.2 GPa axial compressibilities are given by

$$a = 8.310(12) - 0.063(3)P \qquad a = 23.5704(18) - 0.0318(4)P.$$

The bulk modulus of the low-pressure phase, calculated from a Birch–Murnaghan fit of five pressure–volume data (assuming $K' = 4$), is 104(3) GPa. The bulk modulus of the high-pressure form, estimated from three pressure–volume data, is approximately 60 GPa. The compressibility of $RbTi_2(PO_4)_3$ thus increases by approximately 70% above 1.7 GPa.

The structure remains rhombohedral at all pressures up to 6.2 GPa, but we observe a distinct break in slope at approximately 1.7 GPa in plots of cell parameters versus pressure. Above 1.7 GPa the compressibility of the a axis increases by more than 80%, while that of c increases by approximately 34%. This phenomenon of increasing compressibility at high pressure has been observed in a number of other framework structures and typically signals the onset of a reversible 'tilt' transition to lower symmetry, such as those in ReO_3 (Schirber *et al* 1984), zeolites (Hazen and Finger 1979, 1984a, Hazen 1983), and sodium tungstate perovskites (Hazen and Finger 1984b).

3.2. Structure refinements

We initiated the room-pressure $RbTi_2(PO_4)_3$ structure refinements with parameters observed by Masse (1970). In addition to the scale factor and eight variable atomic coordinates, we refined anisotropic temperature factors and an extinction parameter (Zachariasen 1967). The room-pressure refinement converged to a weighted R ($R_w = \Sigma\sigma_F^{-2}(F_o - F_c)^2/\Sigma\sigma_F^{-2}F_o^2$) of 0.029, and unweighted R ($R = \Sigma\|F_o| - |F_c\|/\Sigma|F_o|$) of 0.033, while the goodness of fit for the anisotropic refinement is 1.06. Refined fractional coordinates are given in table 2, and magnitudes and orientations of thermal vibration ellipsoids appear in table 3.

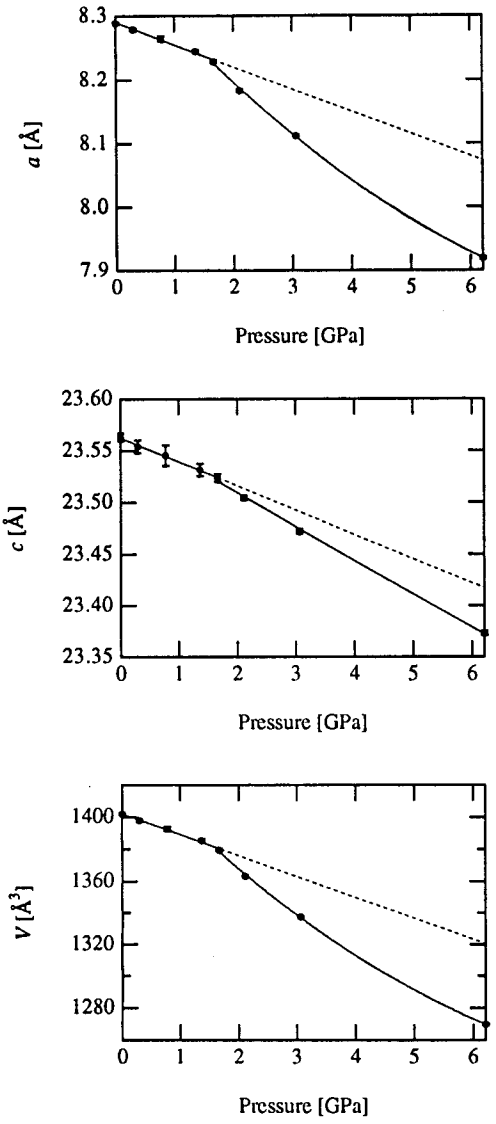

Figure 2. Plots of $RbTi_2(PO_4)_3$ unit-cell parameters a and c (in the hexagonal setting) and unit-cell volume versus pressure show sudden changes in slope at approximately 1.7 GPa.

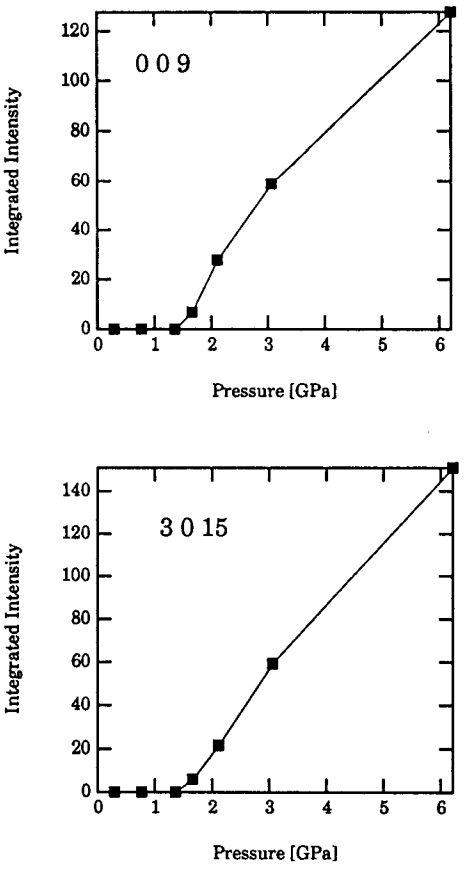

Figure 3. The intensities of the $RbTi_2(PO_4)_3$ (0 0 9) and (3 0 15) reflections (both c-glide violations) versus pressure reveal the onset of a phase transition at approximately 1.7 GPa. Intensities are zero below the transition, and increase continuously and approximately linearly above about 1.7 GPa.

The 6.2 GPa structure refinement was attempted in the centric space group $R\bar{3}$ and in the acentric group $R3$. The structure in the latter space group, with 16 atoms in the asymmetric unit (35 variable positional parameters) yielded significantly better results, with individual parameters deviating by as much as 18 estimated standard deviations from their centric positions. Compare, for example, the x coordinates of the two symmetrically distinct P atoms: 0.7032(11) versus −0.7234(11). In the centric space group the absolute values

Table 2. Conditions of refinement, refined fractional coordinates, and equivalent isotropic thermal parameters for $RbTi_2(PO_4)_3$ at room pressure. Diffraction experiment comprised a Rigaku AFC-5 diffractometer, a rotating-anode generator, Mo $K\alpha_1$ radiation, graphite monochromator, $\lambda = 0.7093$ Å, ω step scans, ambient pressure and temperature. $a = 8.239(1)$ Å, $c = 23.563(1)$ Å, $V = 1402.1$ Å^3; extinction = $3.0(1) \times 10^{-4}$ (Zachariasen 1967); space group $R\bar{3}c$; $Z = 6$; molecular mass = 466.18 g; $\rho_{calc} = 3.312$ g cm^{-3}; $\mu_l = 73.0$ cm^{-1}; $R = \Sigma||F_0| - |F_c||/\Sigma|F_0| = 0.029$, $R_w = \Sigma\sigma_F^{-2}(F_0 - F_c)^2/\Sigma\sigma_F^{-2}F_0^2 = 0.033$ for 459 independent data; largest shift/error = 0.01 in final cycle. Goodness of fit = 1.06 for anisotropic thermal factors.

Atom	x	y	z	β_{11}[a]	β_{22}	β_{33}	β_{12}	β_{13}	β_{23}	B_{eq}
Rb	0	0	0	112(1)[b]	$=\beta_{11}$	2.6(1)	$=\beta_{11}/2$	0	0	1.74(2)
Ti	0	0	0.151 43(2)	18(1)	$=\beta_{11}$	1.6(1)	$=\beta_{11}/2$	0	0	0.37(1)
P	0.719 68(7)	1/4	0	18(1)	19(1)	2.0(1)	$=\beta_{22}/2$	0.4(1)	$=2\beta_{13}$	0.40(2)
O1	0.302 58(20)	0.466 50(19)	0.268 50(6)	63(2)	32(2)	3.4(2)	28(2)	−3.5(5)	−4.5(5)	0.87(3)
O2	0.146 97(19)	0.212 31(18)	0.199 36(6)	46(2)	36(2)	3.2(2)	16(2)	−5.4(5)	−4.0(5)	0.85(3)

[a] Anisotropic thermal parameters $\times 10^4$.

[b] Parenthesized figures represent estimated standard deviation (1σ).

Table 3. Magnitudes and orientations of thermal ellipsoids for $RbTi_2(PO_4)_3$ at room conditions.

Atom	Axis	RMS amplitude (Å)	Angle (°) with respect to *a* axis	*b* axis	*c* axis
Rb	1	0.085(2)	90	90	0
	2	0.1713(6)	—[a]	—	90
	3	0.1713(6)	—	—	90
Ti	1	0.068(3)	90	90	0
	2	0.068(2)	—[a]	—	90
	3	0.068(2)	—	—	90
P	1	0.068(2)	90(72)	40(58)	119(6)
	2	0.069(3)	57(4)	128(4)	42(4)
	3	0.078(2)	90(5)	66(7)	29(6)
O1	1	0.069(4)	102(3)	38(4)	55(4)
	2	0.104(3)	57(4)	128(4)	42(4)
	3	0.132(2)	36(4)	90(3)	111(3)
O2	1	0.069(4)	71(3)	69(3)	43(3)
	2	0.109(3)	63(6)	155(5)	65(5)
	3	0.125(3)	34(6)	104(6)	122(4)

[a] Atom is uniaxial; therefore, principal angles in section of ellipsoid $\perp c$ are undefined.

of these two parameters would be equal. Similarly, the z coordinate of RbB is 0.5033(4)—eight standard deviations from the 0.5 constrained value of space group $R\bar{3}$. Refinement in space group $R3$ converged to a weighted R of 0.083, and unweighted 0.123 for all 526 independent data; $R = 0.080$, $R_w = 0.088$ for 412 data with $F_0 > 2\sigma_F$. Refined fractional coordinates and isotropic temperature parameters are listed in table 4. Tables of observed and calculated structure factors are available from the authors.

4. Discussion

4.1. The phase transition

The structure appears to remain rhombohedral as a function of pressure up to 6.2 GPa, but several changes at about 1.7 GPa signal the onset of a reversible phase transition at about that pressure.

(1) Plots of cell parameters versus pressure reveal a distinct downward break in slope, indicative of increased compressibility, at about 1.7 GPa. These data also suggest the possibility of a slight volume discontinuity at 1.7 GPa if one assumes that the pressure dependence is linear. It seems more likely, however, that the volume shows a curved path of decreasing slope with increased pressure, which would be consistent with a continuous nature for the phase transition. More pressure–volume data in the vicinity of the transition are required to resolve this issue.

(2) At pressures greater than 1.7 GPa violations of the c glide appear. The significant intensities of reflections (0 0 9) and (3 0 15) as illustrated in figure 3, for example, indicate a phase transition from $R\bar{3}c$ to a lower-symmetry rhombohedral space group. Furthermore, the continuous nature of these intensities versus pressure, as well as their approximately linear trend, is evidence for the near second-order nature of the transition.

(3) We observe a sharp drop in the absolute intensities of several strong reflections, including the (3 0 12) and ($\bar{3}$ 0 15), near the 1.7 GPa transition (figure 4). Perhaps this feature is related to a sharp increase in diffuse scattering near the transformation.

Table 4. Conditions of refinement, refined fractional coordinates, and isotropic thermal parameters for $RbTi_2(PO_4)_3$ at 6.2 GPa. The diffraction experiment was carried out with a Picker automated diffractometer, Nb-filtered Mo Kα radiation, λ = 0.7093 Å, ω step scans, 6.21(5) GPa pressure, and room temperature. a = 7.9200(8) Å, c = 23.373(1) Å, V = 1269.68(26) Å^3; extinction = 2.3(1) × 10^{-4}; space group $R3$; Z = 6; molecular mass = 466.18 g; ρ_{calc} = 3.658 g cm^{-3}; μ_l = 80.6 cm^{-1}; $R = \Sigma||F_0| - |F_c||/\Sigma|F_0| = 0.089$, $R_w = \Sigma\sigma_F^{-2}(F_0 - F_c)^2/\Sigma\sigma_F^{-2}F_0^2 = 0.049$ for 504 independent data; R = 0.061, R_w = 0.046 for 394 data with $F_0 > 2\sigma_F$. Largest shift/error = 0.03 in final cycle. Goodness of fit = 1.09 for this refinement.

Atom	x	y	z	B
Rb A	0	0	0	1.04(4)[a]
Rb B	0	0	0.5033(4)	1.22(5)[a]
Ti A	0	0	0.1505(6)	0.36(4)[b]
Ti B	0	0	−0.1480(6)	—
Ti C	0	0	0.6554(5)	—
Ti D	0	0	−0.6510(5)	—
P A	0.7032(11)	−0.0083(11)	0.2528(6)	0.22(5)[b]
P B	−0.7234(11)	−0.0057(11)	−0.2493(6)	—
O1 A	0.2405(27)	0.4334(28)	0.2778(8)	0.67(11)[b]
O1 B	0.4822(25)	0.3550(22)	0.2392(8)	—
O1 C	−0.2400(27)	−0.4585(28)	−0.2694(9)	—
O1 D	−0.5179(26)	−0.4013(22)	−0.2349(8)	—
O2 A	0.1855(23)	0.2035(27)	0.1964(8)	0.74(2)[b]
O2 B	0.2238(28)	0.1413(28)	0.3024(8)	—
O2 C	−0.1525(24)	−0.2189(26)	−0.1948(8)	—
O2 D	−0.2369(28)	−0.1224(27)	−0.2920(8)	—

[a] The Rb A and Rb B atoms were refined as anisotropic. For Rb A, $\beta_{11} = \beta_{22} = 2\beta_{12}$ = 0.0063(4); β_{33} = 0.000 34(5); $\beta_{13} = \beta_{23} = 0$. For Rb B, $\beta_{11} = \beta_{22} = 2\beta_{12}$ = 0.0084(5); β_{33} = 0.000 22(6); $\beta_{13} = \beta_{23} = 0$.

[b] All isotropic temperature factors for Ti, P, O1, and O2 were constrained to be equal.

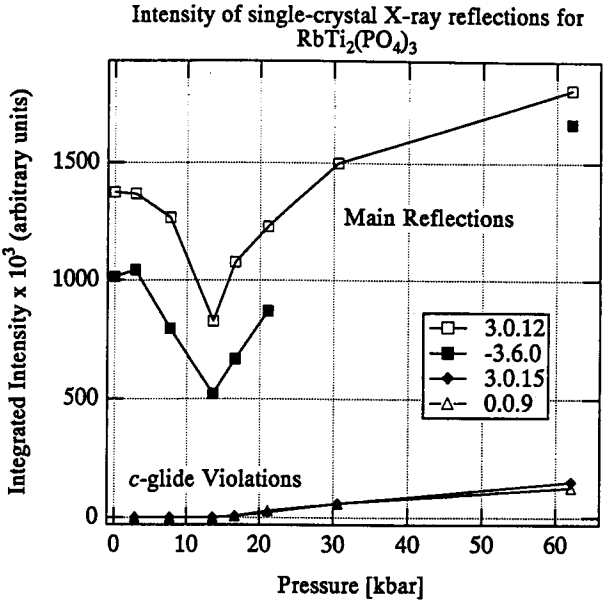

Figure 4. Absolute intensities of main $RbTi_2(PO_4)_3$ reflections decrease sharply near the 1.7 GPa transition.

4.2. High-pressure structural changes

While the nature of the high-pressure phase transition is defined by the pressure dependence of the lattice parameters and the intensities of critical reflections, the nature of accompanying structural changes is revealed by comparison of the $RbTi_2(PO_4)_3$ structure at room pressure and 6.2 GPa. The major structural change that produces the 10% volume compression of $RbTi_2(PO_4)_3$ between room pressure and 6.2 GPa is evident in (001) projections at these two pressures (figure 5). The figure highlights rotation of Ti octahedra and consequent collapse of the Ti–P framework in this plane. This octahedral rotation takes place primarily about the c axis, which leads to the significantly greater compressibility of a compared to c.

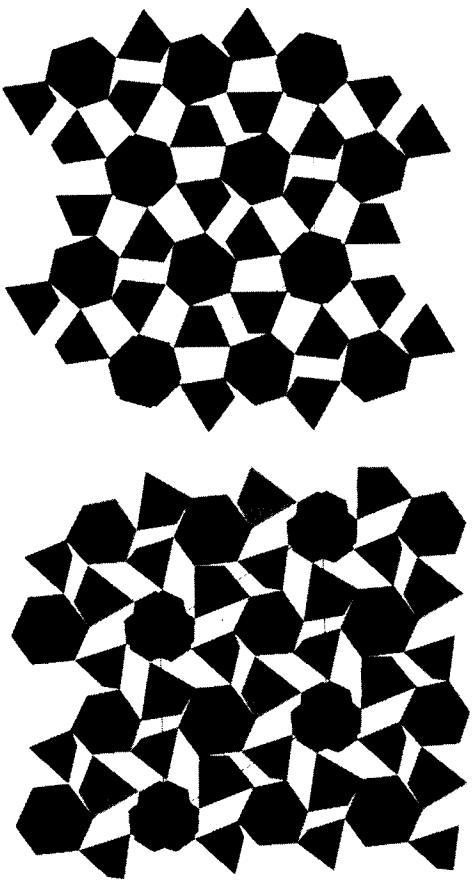

Figure 5. Major high-pressure structural changes are evident in a (001) projection (the b axis is vertical), with corner-linked P tetrahedra and Ti octahedra shown as polyhedra and Rb ions as black circles. The upper view shows the relatively open structure at room pressure. The lower view of the structure at 6.2 GPa highlights rotation of octahedra and collapse of the framework in the (001) plane.

Comparison of the $RbTi_2(PO_4)_3$ structure at room pressure and 6.2 GPa reveals several significant changes in bond distances and angles (table 5), all of which are typical of the compression of corner-linked frameworks. Unfortunately, O fractional coordinates for the high-pressure refinement are poorly constrained—a common difficulty in heavy-atom structures with the restricted high-pressure data set. Nevertheless, while individual cation–O bond distances are less precisely constrained for the high-pressure phase, the mean Ti–O and P–O distances are better defined. The framework-forming Ti octahedra and P tetrahedra show little change in Ti–O and P–O distances with pressure. At room pressure values are

Table 5. Selected interatomic distances and bond angles for $RbTi_2(PO_4)_3$ at room pressure and at 6.2 GPa.

Room pressure		6.2 GPa			
Atoms	Distance	Atoms	Distance	Atoms	Distance
P–O1[2][a]	1.523(1)	P A–O1 A	1.44(2)	P B–O1 C	1.70(2)
P–O2[2][a]	1.530(1)	P A–O1 B	1.40(2)	P B–O1 D	1.65(2)
Mean P–O	1.527	P A–O2 A	1.53(2)	P B–O2 C	1.56(2)
		P A–O2 B	1.58(2)	P B–O2 D	1.48(2)
		Mean P A–O	1.49	Mean P B–O	1.60
			Mean P–O = 1.54		
Ti–O1[3]	1.939(1)	Ti A–O1 D[3]	1.947(19)	Ti B–O1 B[3]	2.000(19)
Ti–O2[3]	1.927(1)	Ti A–O2 A[3]	1.881(18)	Ti B–O2 C[3]	1.888(19)
Mean Ti–O	1.933	Mean Ti A–O	1.914	Mean Ti B–O	1.944
		Ti C–O1 A[3]	1.915(20)	Ti D–O1 C[3]	1.823(21)
		Ti C–O2 D[3]	2.039(19)	Ti D–O2 B[3]	1.897(19)
		Mean Ti C–O	1.977	Mean Ti D–O	1.860
			Mean Ti–O = 1.924		
Rb–O1[6]	2.855(1)	Rb A–O1 B[3]	2.694(19)	Rb B–O1 A[3]	2.992(19)
Rb–O2[6]	3.368(1)	Rb A–O1 D[3]	2.758(19)	Rb B–O1 C[3]	2.860(20)
		Rb A–O2 B[3]	3.132(19)	Rb B–O2 A[3]	3.303(18)
		Rb A–O2 D[3]	3.103(19)	Rb B–O2 C[3]	3.176(18)
Mean Rb–O		Mean Rb A–O		Mean Rb B–O	
for 6	2.855	for 6	2.726	for 6	2.926
for 12	3.112	for 12	2.922	for 12	3.090
			Mean Rb–O = 2.826[6], 3.006[12]		
			Ti–O–P angles (°)		
Ti–O1–P	159.5(1)	Ti C–O1 A–P A	146(1)	Ti A–O2 A–P A	155(1)
Ti–O2–P	143.5(1)	Ti B–O1 B–P A	147(1)	Ti D–O2 B–P A	137(1)
		Ti D–O1 C–P B	141(1)	Ti B–O2 C–P B	140(1)
		Ti A–O1 D–P B	128(1)	Ti C–O2 D–P B	126(1)
Mean Ti–O–P	151.5		Mean Ti–O–P = 140		

[a] Bracketed figures represent bond multiplicities.

1.93 and 1.53 Å, while those at 6.2 GPa are 1.92 and 1.54 Å, respectively. These units thus appear to act as rigid elements of the structure.

Angles between corner-linked tetrahedra and octahedra as measured by Ti–O–P bond angles, on the other hand, change significantly, from an average value of 151.5° at room pressure to 140° at 6.2 GPa. The collapse of these angles provides the principal compression mechanism for $RbTi_2(PO_4)_3$.

Rubidium cations, which occupy cavities in the framework, are effectively six coordinated (Rb–O = 2.86 Å) at room pressure. The distortion of the Ti–P framework causes these cavities to collapse around the Rb cations, increasing their effective coordination to twelve (Rb–O = 3.01 Å) at high pressure. Rubidium thermal vibration ellipsoids at both room pressure and 6.2 GPa are highly anisotropic, with RMS amplitudes approximately twice as large in the (001) plane as parallel to the *c* axis. An interesting feature of these refinements is significant decrease in Rb vibration amplitudes with pressure: B_{EQ} drops from 1.74(2) at room pressure to a mean of 1.13(4) at 6.2 GPa. Ti and O vibration amplitudes, on the other hand, are unchanged within errors. This large decrease may reflect the increasingly constrained environment of Rb at pressure.

High-pressure structural changes in $RbTi_2(PO_4)_3$ are similar to those observed by Allan *et al* (1992) in $KTiPO_5$. The principal changes in the latter compound between room

pressure and 4.7 GPa include reduction of all Ti–O–P angles from a mean value of 132.7 to 131.1° and reduction of mean K–O distance from 2.889 to 2.856 Å. Allan *et al* also found that P tetrahedra and Ti octahedra are essentially unchanged in size or shape at pressures of several GPa.

5. Conclusions

The acentric high-pressure phase of $RbTi_2(PO_4)_3$ is especially intriguing because of the key role Ti phosphates play as non-linear optic materials. It may be possible to use element substitutions to produce the acentric variant at room conditions.

$KTiPO_5$ and its acentric isomorphs in space group $Pna2_1$ are widely used in laser frequency doublers and for other applications (Phillips *et al* 1992). That structure, like high-pressure $RbTi_2(PO_4)_3$, features a near-centric, corner-linked array of Ti octahedra and P tetrahedra with interstitial alkali cations. Several isomorphs of $KTiPO_5$, including $KGeAsO_5$ and $KGePO_5$, occur in the centric space group $Pnam$; it seems likely that these compounds transform to the acentric $Pna2_1$ form at high pressure. Thus, given the similarities of $KTiPO_5$ and $RbTi_2(PO_4)_3$, efforts should be made to synthesize and examine an isomorph of the acentric $RbTi_2(PO_4)_3$ structure at room pressure.

The observed reduction of Ti–O–P angles, and the concomitant collapse of the alkali sites at high pressure, point to substitution of a smaller alkali cation, such as Na or Li for Rb, as the most promising path to such synthesis. In fact, Masse (1970) described the synthesis of both polycrystalline $LiTi_2(PO_4)_3$ and $NaTi_2(PO_4)_3$. He assumed the centric space group $R\bar{3}c$ in his description, though small deviations to $R\bar{3}$ or $R3$ would have been indistinguishable from his data. Curiously, Masse found that substitution of smaller alkali cations leads to a sharp reduction of the c axis, but a slight increase in a, so that the rhombohedral angle approaches 60° with the smallest alkali cation, Li. These observations contrast with the pressure results on $RbTi_2(PO_4)_3$, in which a compresses much more than c. It appears, therefore, that increasing pressure and substitution of smaller alkali cations, while both causing dramatic reductions in molar volume, produce very different changes in the $RbTi_2(PO_4)_3$ structure.

Efforts to produce and examine single crystals of $RbTi_2(PO_4)_3$ isomorphs are now under way.

Acknowledgments

This work was supported by the National Science Foundation Center for High-Pressure Research and the Carnegie Institution of Washington, as well as NSF grants DMR9208511 (for crystal synthesis), EAR9117433 (for the study of phase transitions in framework materials), and EAR9218845 (for x-ray crystallography).

References

Allan D R, Loveday J S, Nelmes R J and Thomas P A 1992 *J. Phys.: Condens. Matter* **4** 2747–60
Allan D R and Nelmes R J 1992 *J. Phys.: Condens. Matter* **4** 2747–60
Angel R J 1992 *Am. Mineral.* **77** 923–9
Downs R T and Palmer D C 1993 *Am. Mineral.* **77** at press
Hazen R M 1976 *Science* **194** 105–7

Hazen R M 1983 *Science* **219** 1065–7
Hazen R M and Finger L W 1979 *Phase Trans.* **1** 1–22
—— 1982 *Comparative Crystal Chemistry* (New York: Wiley)
—— 1984a *J. Appl. Phys.* **56** 1838–40
—— 1984b *J. Appl. Phys.* **56** 311–13
King H E and Finger L W 1979 *J. Appl. Crystallogr.* **12** 374–8
Mao H K, Bell P M, Shaner J W and Steinberg D J 1978 *J. Appl. Phys.* **49** 3276–83
Masse R 1970 *Bull. Soc. Fr. Minéral. Cristallogr.* **93** 500–503
Megaw H D 1973 *Crystal Structures: A Working Approach* (Philadelphia, PA: Saunders)
Merrill L and Bassett W A 1974 *Rev. Sci. Instrum.* **45** 290–4
Palmer D C and Downs R T 1991 *EOS Trans. Am. Geophys. Union* **72** 478
Palmer D C and Finger L W 1994 *Am. Mineral.* at press
Palmer D C, Finger L W and Hemley R J 1992 *EOS Trans. Am. Geophys. Union* **73** 521
Phillips M L F, Harrison W T A, Stucky G D, McCarron E M, Calabrese J C and Gier T E 1992 *Chem. Mater.* **4** 222–33
Ralph R L and Finger L W 1982 *J. Appl. Crystallogr.* **15** 537–9
Schirber J E, Morosin B, Alkire R W, Larson A C and Vergamini P J 1984 *Phys. Rev.* B **29** 4150–2
Wang Y, Weidner D J, Liebermann R C, Liu X, Ko J, Vaughan M T, Zhao Y, Yeganeh-Haeri A and Pacalo R E G 1991 *Science* **251** 410–13
Zachariasen W H 1967 *Acta Crystallogr.* **23** 558–64
Zumsteg F C, Berlein J D and Geir T E 1976 *J. Appl. Phys.* **47** 4980–5